Preparation and Characterization of Wood-based Pre-oxidized Precursors and Activated Carbon Microspheres

Junbo Shang,[a,b] Jian Lin,[a,b,*] and Guangjie Zhao [a]

Wood-based activated carbon microspheres (WACMs) were successfully prepared from Chinese fir. However, the weak thermal stability of the precursors resulted in melting at high activation temperatures, which led to a lower yield and poor adsorption properties. To promote the thermal stability of the precursors in the process without chemicals, this paper focused on the effects of the pre-oxidation before activation on the thermal stability and chemical structure of the precursors and the pore structure of the activated samples. The results showed that during the pre-oxidation process, the O/C ratio increased noticeably and the intensity of oxygen-containing functional groups, such as carbonyl, carboxyl, and ester groups, were enhanced, which contributed to the improvement of the thermal stability. Moreover, the etching effect of oxygen on the structure of the precursors was verified when the porous structure was enriched by activation. The activated sample pre-treated at pre-oxidation temperature 250 °C had the maximum micropore specific surface area and pore volume. As the temperature was raised to 280 °C, the mesopore specific surface area and pore volume increased, which indicated that the optimization of the pre-oxidation parameters contributed to the formation of the mesopore structure.

Keywords: Liquefied wood; Thermal stability; Pre-oxidation; Pore structure; Activated carbon microspheres

*Contact information: a: Beijing Key Laboratory of Wood Science and Engineering, Beijing Forestry University, Beijing 100083, China; b: MOE Key Laboratory of Wooden Material Science and Application, Beijing Forestry University, Beijing 100083, China; *Corresponding author: linjian0702@bjfu.edu.cn*

INTRODUCTION

Activated carbon microspheres are widely used in the fields of supercapacitors (Wang *et al*. 2014), adsorption (Martín *et al*. 2011; Wickramaratne and Jaroniec 2013), medicine (Ye *et al*. 2008), heavy metal adsorption (Chen *et al*. 2011), and others, because of its advantages, such as its smooth surface, high packing density, high mechanical strength, good uniformity, rolling property, low flow resistance, *etc.* (Shen *et al*. 2008). Most raw materials used for activated carbon microspheres are prepared from fossil resources, such as pitch, coal, phenolic resin, *etc.* Environmental concerns have prompted researchers to seek alternative raw materials for the preparation of activated carbons from biomass materials, such as wood (Liu *et al*. 2017), lignin (Li *et al*. 2016), and hemp (Guo *et al*. 2016).

Sawdust from wood processing is a readily available biomass resource for value-added utilization. As one of the utilization methods, wood liquefaction and its products can be used to prepare fuels, adhesives, foams, molded products and so on (Pan *et al.* 2009). Moreover, wood-based carbon fibers have been successfully prepared from Chinese fir from liquefied wood (Ma and Zhao 2011; Shang *et al*. 2015), as well as wood-based

activated carbon fibers (Huang *et al*. 2015). For some specific applications, such as fluidized beds and water treatment devices, the advantages of spherical activated carbons are obvious (Shen *et al*. 2008). Moreover, further study on the structure of wood-based carbon materials has indicated that liquefied wood is more suitable for preparing porous structural carbons (Liu *et al*. 2015). However, the most difficult problem has been the low activation yield and small porous structure, which is a result of the low thermal stability of the precursors from liquefied wood (Lin *et al*. 2013).

Pre-oxidation is a requisite process for preparing carbon fibers before carbonization, with no chemicals added. The process is widely used in the preparation of pitch-based carbon fibers. During the pre-oxidation process, a series of complicated reactions, such as cyclization, cross-linking, dehydrogenation, and oxidation of the molecular chains, occur under the conditions of air or oxygen between 200 °C to 400 °C (He 2010). A partial condensation reaction has been found to occur along with removal reactions during pre-oxidation, which leads to more cross-linked reactions and a denser structure (Sun *et al*. 2017). Moreover, after the pre-oxidation treatment, the C1s peak of activated carbons shifts to a higher binding energy, the number of oxygen-containing functional groups increases, and more bonds appear between oxygen and the carbon matrix, which leads to high heat resistance (Liu *et al*. 2011). However, decomposition and crosslinking reactions both occur during the pre-oxidation treatment, mainly because the improper pre-oxidation parameters result in an etching effect of oxygen on the pore walls of the precursors (Liu *et al*. 2010).

To improve the thermal stability of the precursors, wood-based activated carbon microspheres were prepared with the pre-oxidation treatment in air at different pre-oxidation temperatures, which was followed with water steam activation in an inert atmosphere. The morphology, chemical composition of the precursors, and the pore structure of the activated samples were analyzed to reveal the relationship between pre-oxidation and the pore structure of the activated carbon microspheres.

EXPERIMENTAL

Materials

Chinese fir (*Cunninghamia lanceolata*) wood was obtained from Fujian province, China. Chemicals such as phenol, phosphoric acid, hexamethylenetetramine (HTMA), hydrochloric acid, and polyvinyl alcohol (PVA) were purchased from Lanyi Chemical Products Corp. (Beijing, China). All of the chemicals mentioned above were used directly without any further purification.

Methods

Preparation of the precursors

A mixture of 25 g of dried Chinese fir powder (20 mesh to 80 mesh) and 100 g of phenol was added to a bottle flask, and 8 g of phosphoric acid (8.0% based on the weight of the phenol) were then added. The flask was immersed in an oil bath, heated rapidly from room temperature to 160 °C, and incubated for 2.5 h. The flask was cooled to room temperature with cool water, and the resultant mixture was filtered through a glass crucible filter (G2, pore diameter of 10 μm to 15 μm) to separate the filtrate from the residue. Subsequently, the filtered residue was put into a solution that was pre-heated to 65 °C, along with 6% PVA (based on the weight of the liquefied wood), and stirred at a speed of

400 rpm for 2 h. The liquefied wood microspheres (LWCMs) were obtained by freeze drying and were then immersed in a solution of hydrochloric acid (4 M) and 5 g/L HTMA, which was incubated at 85 °C for 2 h. After the treatment, the LWCM was washed with distilled water and dried in a vacuum oven (degree of vacuum = 0.1 MPa) at 45 °C.

The wood-based pre-oxidized microspheres (LWOMs) were prepared by heating the LWCM to 190 °C, 220 °C, 250 °C, 280 °C, and 310 °C at a heating rate of 1 °C/min, and were incubated for 1 h under an air atmosphere. Then, the temperature in the furnace was gradually decreased to room temperature. The samples were marked as LWOM-Tx, where x is the pre-oxidation temperature.

Preparation of the wood-based activated carbon microspheres

The WACMC was prepared using the LWCM, which was first carbonized at 600 °C at a heating rate of 4 °C/min under N_2 and incubated for 1 h. Then, the temperature was increased from 600 °C to 800 °C at a heating rate of 4 °C/min and they were incubated for 1 h under N_2 and water steam.

The LWOMs were placed in an activation furnace and heated to 800 °C under N_2 (flow rate = 100 mL/min) at a heating rate of 4 °C/min. Then, water vapor was introduced at a flow rate of 3.12 g/min and the LWOMs were incubated for 1 h. After the temperature decreased to room temperature, the wood-based activated carbon microspheres pre-treated with pre-oxidation (WACMOs) were obtained and marked as WACMO-Tx, where x is the pre-oxidation temperature.

Characterization

Thermo-gravimetric analysis

The weight loss behaviors and decomposition temperature of the samples were determined by using a thermo-gravimetric analysis (TGA) device (TGA STA449F3, Netzsch Corp., Selb, Germany) from room temperature to 800 °C at a heating rate of 10 °C/min in high-purity argon (flow rate = 60 mL/min).

Fourier transform infrared spectroscopy

Fourier transform infrared (FTIR) spectroscopy of the samples was performed using a FTIR spectrophotometer (Tensor 27, Bruker Corp., Karlsruhe, Germany). The samples were dried before they were mixed with water-removed KBr crystals. This mixture was put in an agate mortar and ground at a weight ratio of 1:100 (sample to KBr crystals). A few samples were pressed on a tablet press to make a transparent sheet for taking measurements. The survey resolution was 4 cm^{-1} with 32 scans and a scanning range of 4000 cm^{-1} to 500 cm^{-1}.

Elemental analysis

Elemental analysis of the samples was performed using an elemental analyzer (FLASH EA1112, Thermo Fisher Scientific Inc., Waltham, USA). The carrier gas was helium, and the applied decomposition temperature of the carbon, hydrogen, and nitrogen was 950 °C.

Scanning electron microscopy

The samples were coated with gold and the morphologies of the samples were observed with scanning electron microscopy (SEM) (S-3400N, Hitachi Corp., Tokyo, Japan) at magnification factors of 1500x to 2000x and an accelerating voltage of 10 kV.

X-ray photoelectron spectroscopy

To determine the number and type of functional groups present on the surface of the samples, X-ray photoelectron spectroscopy (XPS) measurements were performed on a spectrophotometer (ESCALAB 250Xi, Thermo Fisher Scientific Inc.) with a monochromated Al Kα X-ray source ($h\nu$ = 1486.6 eV) and a power of 420 W. The survey scans were collected from the binding energy range of 0 eV to 1350 eV. A nonlinear, least squares regression analysis program (XPSPEAK software, Version 4.1., Informer Technologies, Inc., Hong Kong, China) was used for the XPS spectral deconvolution.

Specific surface area and pore structure analysis

The N_2 adsorption-desorption isotherms were measured at 77 K with a surface area and porosity analyzer (Autosorb-IQ, Quantachrome Instruments Corp., Boynton Beach, FL, USA). The samples were out-gassed at 300 °C for 3 h before taking measurements to remove any moisture or volatile compounds within the pores of the samples. The Brunauer-Emmett-Teller (BET) model was used to calculate the surface area (S_{BET}) of the N_2 adsorption isotherms over the relative pressure (P/P_0) range of 0.05 to 0.3 (Okada *et al*. 2003). The adsorption total pore volumes at relative pressures of 0.1 and 0.995 are equal to the volume of the micropores and total volume of the micropores and mesopores (V_{tot}), respectively (Nabais *et al*. 2004; Azargohar and Dalai 2008). The micropore (S_{micro}) and mesopore areas (S_{meso}) were calculated according to the t-plot and Barrett-Joyner-Halenda methods, respectively. The pore size distribution was calculated using the density functional theory method (Lastoskie *et al*. 1993).

RESULTS AND DISCUSSION

Thermal Stability of the LWCM and LWOMs

The thermo-gravimetric (TG) and differential thermo-gravimetric (DTG) curves of the LWCM and LWOMs prepared at different pre-oxidation temperatures are shown in Fig. 1. Figure 1a shows that the pyrolysis weight loss rate of all of the samples during the first stage from room temperature to 100 °C was less than 5%, which was mainly because of the evaporation of water. From 100 °C to 250 °C there was a pyrolysis reaction that occurred in the LWCM, but there was no obvious weight loss during this stage, which indicated that there were few pyrolysis reactions that occurred in the LWOMs. The fastest pyrolysis weight loss reaction occurred from 300 °C to 700 °C, and the by-products, such as low molecular weight phenolic substances (CH_4, CO, and CO_2), combusted or evaporated as the temperature increased (Zhang and Shen 2009). The end of the pyrolysis stage occurred from 700 °C to 800 °C. During this stage, the weight loss rate decreased gradually and only a few small molecular substances continued decomposing.

Although the variation in the TG curves between the different pre-oxidation temperatures was not obvious, the promotion of pre-oxidation to reduce the pyrolysis rate was distinctive, and the minimum pyrolysis residual rate of all of the samples prepared by pre-oxidation was 48.8%, which was greater than that of the LWCM. Therefore, even there was small pyrolysis loss under the conditions of air and heat, the effect of the pre-oxidation on improving the thermal stability of the precursors was more obvious. Meanwhile, the subsequent activation process was simplified.

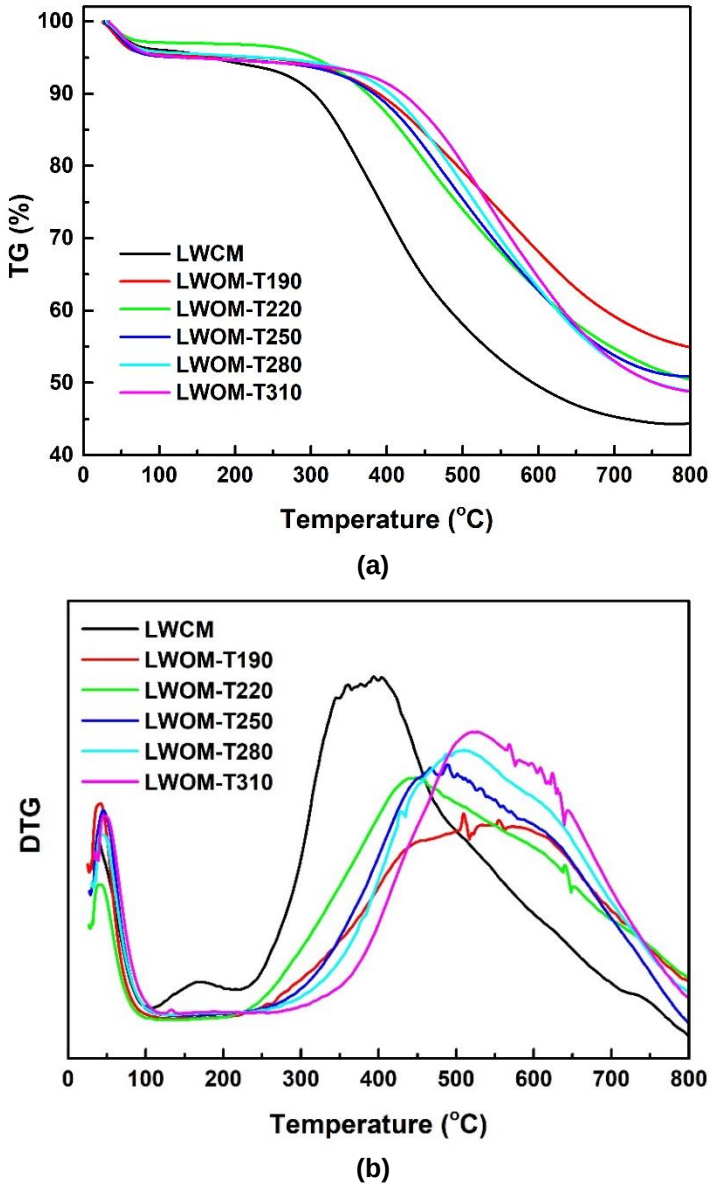

Fig. 1. TG (a) and DTG (b) curves of the LWCM and LWOMs prepared at different pre-oxidation temperatures

Figure 1b shows that the differences in the maximum pyrolysis reaction rate between the LWCM and LWOMs during the pyrolysis process were obvious, especially when the pyrolysis temperature was higher than 100 °C. From 100 °C to 200 °C, the DTG curve of the LWCM fluctuated more than those of the LWOMs, and the maximum pyrolysis reaction rate of the LWCM was more concentrated. Moreover, as the pre-oxidation temperature increased, the peak pyrolysis temperature shifted to a higher temperature. The maximum peak temperature appeared at 527 °C with LWOM-T310, which was higher than that of the LWCM. Therefore, the DTG curves illustrated that the molecular crosslinking degree of the LWOMs was enhanced and the thermal resistance became stronger as the pre-oxidation temperature increased.

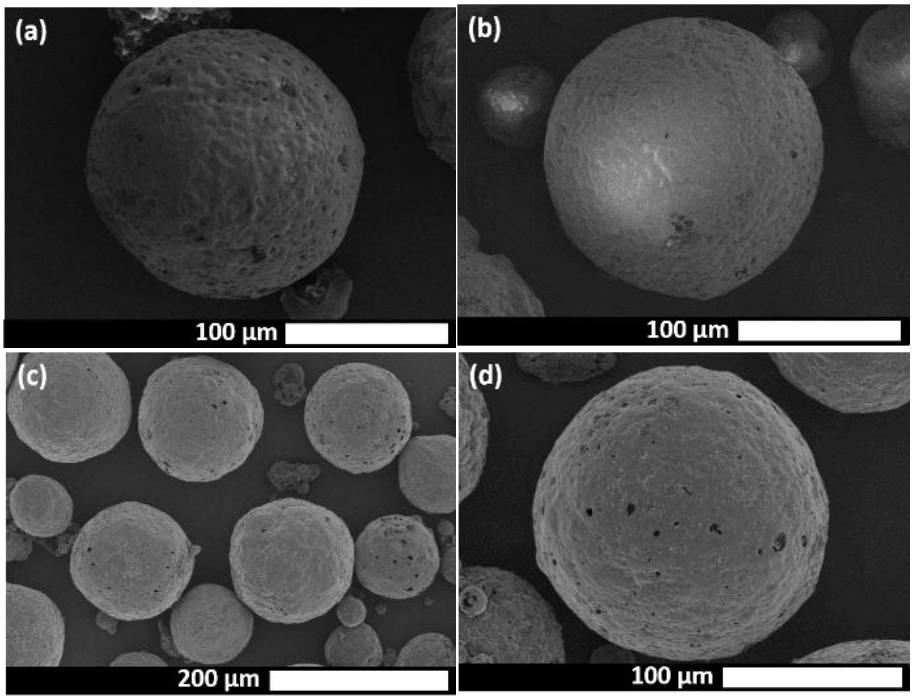

Fig. 2. SEM images of the LWCM (a) and LWOM-T250 (b) at 500x magnification, WACMO-T250 (c) at 250x magnification, and WACMO-T250 (d) at 500x magnification

Figure 2 depicts the morphologies of the LWCM, LWOM-T250, and WACMO-T250. The chemical curing and pre-oxidation treatment had few effects on the spherical shape of the microspheres, but the chemical curing process formed a dense solidified layer on the surface of the LWCM (Ma and Zhao 2010). After the pre-oxidation treatment, the surface of the LWOM-T250 became smoother and denser than before. Because the pre-oxidation treatment resulted in a dense surface layer with few pores, further processes, such as carbonization and activation, were necessary to open the inner and outer pore connections. During the activation process, the internal pore structure was enriched and the connections between the surface and inner pores were opened. More pores were observed on the surface of the activated samples, mainly because of the etching effects of the water steam and high temperature used during activation.

Cross-linking Reaction during Pre-oxidation

Figure 3a shows the FTIR spectra of the LWCM and LWOMs prepared at different pre-oxidation temperatures. The adsorption peak from 3400 cm^{-1} to 3430 cm^{-1} was attributed to the -OH vibration frequencies of hydroxyl groups (Silverstein *et al*. 2005), which became wider and weaker as the pre-oxidation temperature increased. The adsorption peaks at 1352 cm^{-1} and 1608 cm^{-1}, that were attributed to benzene rings, were diminished after pre-oxidation. Meanwhile, the intensity of the peaks at 1454 cm^{-1}, which were attributed to the C-H stretching of methylene groups, and the peaks at 830 cm^{-1} and 756 cm^{-1}, which were attributed to C-H vibration, showed a decreasing trend as well. This manifested when the hydrocarbon functional groups were combusted or oxidized during the pre-oxidation process. In contrast, the adsorption peak at 1703 cm^{-1}, which was assigned to the keto, carbonyl, and ester groups, was enhanced noticeably, and the peak moved to higher frequencies as the pre-oxidation temperature increased. This indicated that a large amount of oxygen-containing functional groups was formed during the pre-

oxidation process. These results were consistent with the variations in the element contents (Fig. 3b).

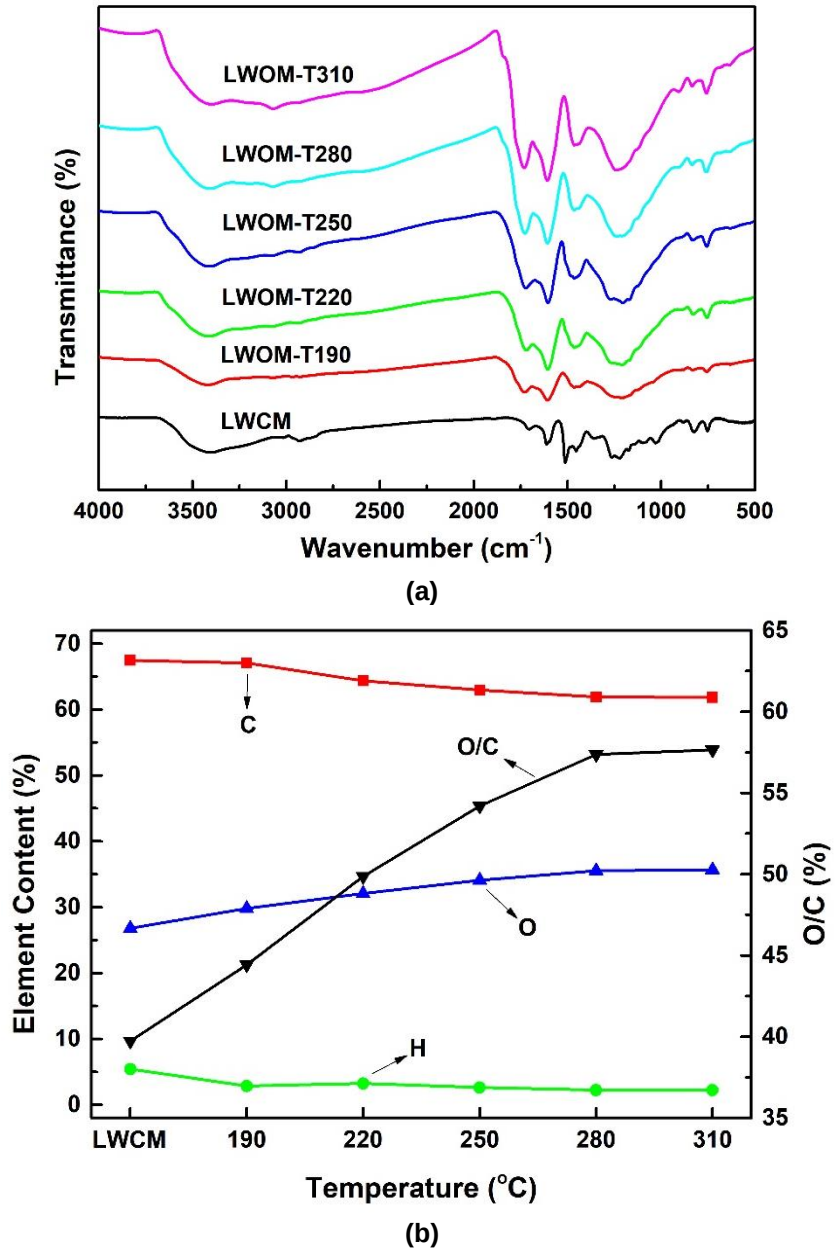

Fig. 3. FTIR spectra (a) and element contents (b) of the LWCM and LWOMs prepared at different pre-oxidation temperatures

The variations in the element contents for the LWCM and LWOMs prepared at different pre-oxidation temperatures are shown in Fig. 3b. Before the pre-oxidation treatment, the relative elemental carbon content was higher than those in the LWOMs, and the oxygen content and O/C ratio were lower than those in the LWOMs. As the pre-oxidation temperature increased, the carbon and hydrogen contents decreased gradually and the oxygen content increased. As a result, the O/C ratio increased noticeably from 39.7% in the LWCM to 57.7% in LWOM-T310, which indicated that the amount of

oxygen-containing functional groups formed during the pre-oxidation process and the amount of aliphatic hydrocarbon functional groups containing carbon and hydrogen were both reduced. However, the oxygen content increase rate from 280 °C and 310 °C was small, which was mainly because the combustion rate of the oxygen-containing functional groups was exceeded by the formation rate under the high temperature condition (Liu *et al*. 2010).

Variation in the Chemical Compositions for the Different Processes

The XPS spectra of the LWCM, LWOM-T250, WACMC, and WACMO-T250 are depicted in Fig. 4a.

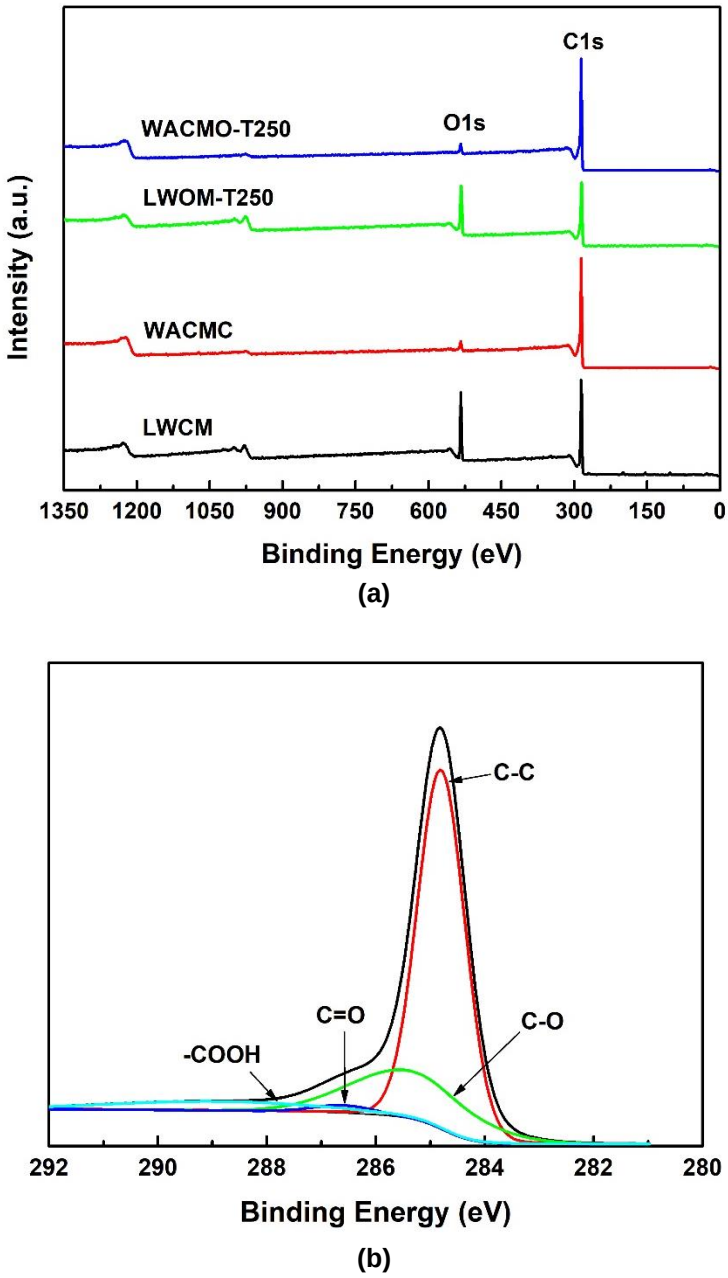

Fig. 4. XPS spectra of the LWCM, LWOM-T250, WACMC, WACMO-T250 (a); peak fitting of the XPS C1s peaks for WACMO-T250 (b)

Table 1 summarizes the elemental compositions on the surface of all of the samples. Carbon was the most abundant constituent in all of the samples and clearly increased after activation. The nitrogen content was the lowest mainly because there were no nitrogen-containing substances that had been introduced during the preparation process, and nitrogen escaped as by-products during activation (Mangun *et al*. 2001). In contrast, the oxygen content increased after the pre-oxidation treatment, mainly because oxygen combined with the LWOMs in the form of bound oxygen, which increased the amount of oxygen-containing functional groups and the oxygen-carbon ratio. Under the conditions of a high activation temperature and water steam, the thermal decomposition of oxygen-containing carbon functional groups released a large amount of carbon and oxygen compounds, which promoted the enrichment of carbon and the pyrolysis of oxygen-containing functional groups.

The C1s spectra of the LWCM, LWOM-T250, WACMC, and WACMO-T250 were similar. Therefore, only the WACMO-T250 spectrum is depicted in Fig. 4b. For all of the samples, the C1s signals showed an asymmetric tailing, which was attributed to the intrinsic asymmetry of the graphite peaks and contribution of oxygen surface complexes. Deconvolution of the four individual component peaks of the C1s spectra was performed and indicated the presence of graphitic carbon (284.6 eV to 284.8 eV); carbon present in alcohol, ether, or C=N groups (285.4 eV to 286.2 eV); carbonyl or quinine groups (286.4 eV to 287.1 eV); and carboxyl, lactone, or ester groups (288.1 eV to 288.9 eV) (Chiang *et al*. 2007).

Table 1. Surface Elemental Composition of the LWCM, LWOM-T250, WACMC, and WACMO-T250

Sample	C1s (%)	O1s (%)	N1s (%)	O/C (%)
LWCM	77.24	21.63	1.04	28.00
LWOM-T250	74.80	24.28	0.92	32.50
WACMC	95.13	4.35	0.52	0.046
WACMO-T250	95.07	4.25	0.67	0.045

Table 2 summarizes the percentages of the graphitic and functional carbon atoms in the samples. Comparison of the spectra was done between the LWCM, LWOM-T250, WACMC, and WACMO-T250. After the pre-oxidation treatment, the relative amount of graphitic carbon and C/O functional groups, such as C-O and carbonyl, were reduced, except for the carboxyl functional groups. Because of the combination with oxygen, the percentage of carboxyl functional groups increased remarkably.

Table 2. Results of the Fits of the C1s regions

Sample	C-C		C-O		C=O		-COOH	
	BE (eV)	RC (%)	BE (eV)	RC (%)	BE (eV)	RC (%)	BE (eV)	RC (%)
LWCM	284.7	60.19	285.6	15.16	286.5	14.63	288.3	10.02
LWOM-T250	284.7	59.38	285.6	5.79	286.5	13.24	288.2	21.59
WACMC	284.8	70.10	285.5	22.19	286.4	1.07	288.9	6.64
WACMO-T250	284.8	68.31	285.4	22.25	286.6	1.78	288.9	7.67
BE – binding energy; RC – relative content								

After activation, the percentage of the carbonate groups both in the WACMC and WACMO-T250 increased noticeably. In contrast, the functional groups C=O and -COOH were reduced greatly, which was mainly because the increasing amounts of graphitic carbons reacted with steam water molecules to generate additional functional groups containing C-O (Lin and Zhao 2016). Furthermore, the carbonyl and carboxyl functional groups were consumed, which resulted in volatile by-products, such as CO_2, CO, and H_2O (Ma *et al*. 2017).

Pore Structure of the WACMC and WACMOs

The N_2 adsorption-desorption isotherms and pore size distribution of the WACMC and WACMOs pre-treated at various pre-oxidation temperatures are shown in Fig. 5. As the pre-oxidation temperature increased from 190 °C to 310 °C, the greatest N_2 adsorption capacity was 350 cm^3/g, which was recorded with the WACMO-T280. The isothermal adsorption/desorption curves showed the same tendency for the different pre-oxidation temperatures. The isotherms increased in the low-pressure zone rapidly, which indicated that the samples had a typical microporous structure. As the pre-oxidation temperature increased, the isotherms of the WACMOs showed a more pronounced knee-like shape and narrower hysteresis loops than the WACMC, which illustrated that there was part of an irregular mesopore structure with a smaller size that existed in the WACMOs (Jin and Huang 2015).

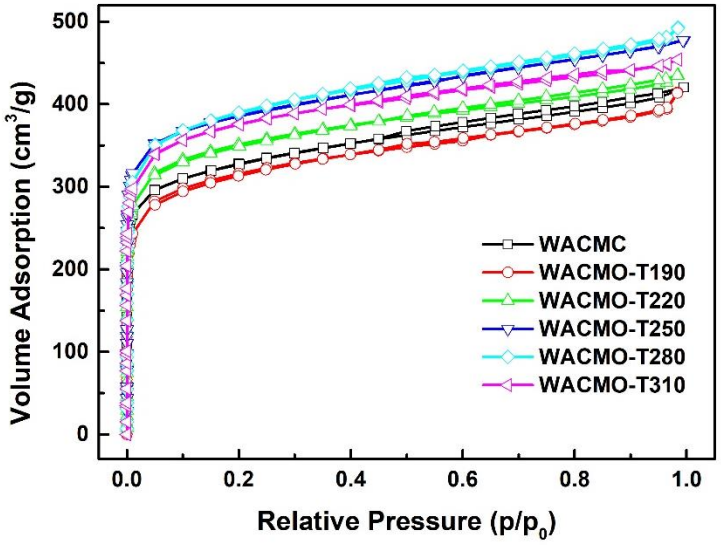

Fig. 5. N_2 adsorption-desorption isotherms at 77 K of the WACMC and WACMOs

The pore size distributions of the WACMC and WACMOs pre-treated at various pre-oxidation temperatures are shown in Fig. 6. Figures 6a and 6b show the micropore and mesopore areas, respectively. The presence of both micropores and mesopores was indicated by the sample curves. The same trend of the pore size distribution showed that the different temperatures had more of an effect on the mesopore size distribution than on the micropore size distribution. The pore size distribution of the micropore area was mainly concentrated in the range of 0.5 nm to 1.4 nm. However, in the mesopore region (2 nm to 30 nm), the pore size distribution was mainly concentrated from 2 nm to 10 nm. Although WACMO-T250 appeared to have a higher integral pore volume when the pore size was

greater than 6 nm, the integral pore volume in the range of 2 nm to 6 nm was less than that of WACMO-T280. Consequently, it was concluded that the appropriate pre-oxidation temperature enriched the mesoporous structure of the samples.

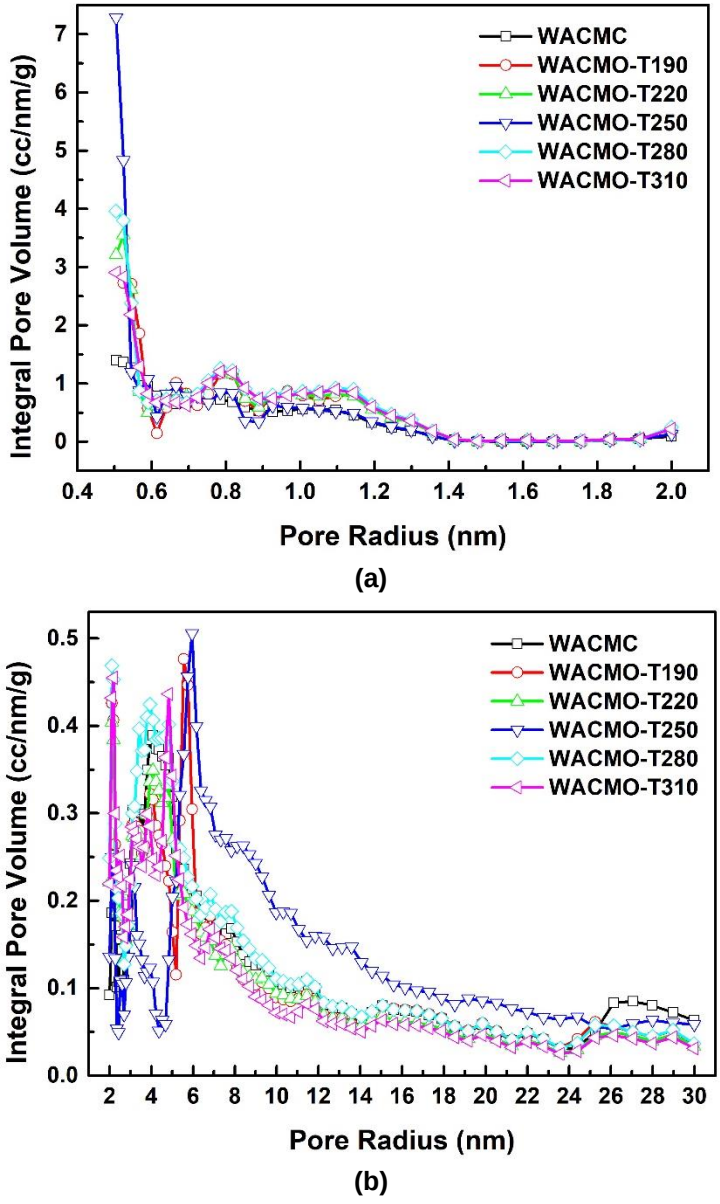

Fig. 6. Pore size distribution of the micropore (a) and mesopore (b) areas of the WACMC and WACMOs

Table 3 summarizes the pore structure parameters of the WACMC and WACMOs pre-treated at various pre-oxidation temperatures. The specific area and pore volume of WACMO-T190 were lower than those of the WACMC. As the pre-oxidation temperature increased, the etching effects of oxygen on the pore structure became more noticeable. The specific area and pore volume of the WACMOs exceeded those of the WACMC, especially the mesopore volume. The pre-oxidation treatment played a large role in promoting the specific surface area and pore volume of the WACMOs, which was mainly because of the etching effect on the inner structure of the precursors during pre-oxidation (Ma *et al*. 2017).

Table 3. Nitrogen Adsorption and Pore Structure Parameters of WACMC and WACMOs

Sample	S_{BET} (m^2/g)	S_{micro} (m^2/g)	V_{micro} (cm^3/g)	S_{meso} (m^2/g)	V_{meso} (cm^3/g)	V_{total} (cm^3/g)
WACMC	1239	982	0.398	191	0.215	0.650
WACMO-T190	1187	953	0.390	179	0.219	0.640
WACMO-T220	1330	1088	0.441	180	0.197	0.673
WACMO-T250	1473	1209	0.484	199	0.217	0.739
WACMO-T280	1469	1177	0.477	219	0.243	0.762
WACMO-T310	1425	1195	0.484	117	0.188	0.703

Among the different samples of the WACMOs, the pore structure value increased at first, and then it decreased as the pre-oxidation temperature increased. Compared with WACMO-T190, the specific surface areas of WACMO-T250 and WACMO-T280 were 1473 m^2/g and 1469 m^2/g, which were increases of 24.1% and 23.8%, respectively. The pre-oxidation temperature of 250 °C contributed to a higher micropore specific area and pore volume, which were 1209 m^2/g and 0.484 cm^3/g, respectively. In contrast, the mesopore specific area and pore volume of the WACMO-T280 reached the maximum values of 219 m^2/g and 0.243 cm^3/g, respectively. The results showed that the pre-oxidation temperature increasing from 190 °C to 250 °C promoted the growth of the micropore specific area and pore volume. Consequently, as the pre-oxidation temperature continued to increase, the etching effect of oxygen on the pore walls of the WACMOs became stronger. As a result, the original microporous structure was destroyed and the mesoporous structure increased (Sun *et al*. 2017). However, excessive temperatures resulted in the collapse of pore walls, which led to a decrease in the specific surface area and pore volume.

CONCLUSIONS

1. The pre-oxidation treatment was successfully applied to enhance the thermal stability of the precursors before activation. After pre-oxidation, the pyrolysis rates of the LWOMs increased remarkably compared with those of the LWCM.
2. As the pre-oxidation temperature increased, the O/C ratio increased noticeably and the intensity of oxygen-containing functional groups, such as carbonyl, carboxyl, and ester groups, was fortified. Meanwhile, the surface layer of the LWOMs became denser because of the pre-oxidation process.
3. The etching effect of oxygen on the pore structure of the WACMOs became stronger as the pre-oxidation temperature increased, which contributed to the formation of the mesopore structure. The maximum mesopore specific surface area and pore volume of WACMO-T280 were 219 m^2/g and 0.243 cm^3/g, respectively.

ACKNOWLEDGMENTS

The authors are grateful for the support of "The Fundamental Research Funds for the Central Universities" (Grant No. 2017PT11).

REFERENCES CITED

Azargohar, R., and Dalai, A. K. (2008). "Steam and KOH activation of biochar: Experimental and modeling studies," *Micropor. Mesopor. Mat.* 110(2-3), 413-421. DOI: 10.1016/j.micromeso.2007.06.047

Chen, Z., Ma, L., Li, S., Geng, J., Song, Q., Liu, J., Wang, C., Wang, H., Li, J., Qin, Z., *et al*. (2011). "Simple approach to carboxyl-rich materials through low-temperature heat treatment of hydrothermal carbon in air," *Appl. Surf. Sci.* 257(20), 8686-8691. DOI: 10.1016/j.apsusc.2011.05.048

Chiang, Y.-C., Lee, C.-C., and Lee, H.-C. (2007). "Characterization of microstructure and surface properties of heat-treated PAN-and rayon-based activated carbon fibers," *J. Porous Mat.* 14(2), 227-237. DOI: 10.1007/s10934-006-9028-8

Guo, N., Li, M., Wang, Y., Sun, X., Wang, F., and Yang, R. (2016). "N-doped hierarchical porous carbon prepared by simultaneous-activation of KOH and NH_3 for high performance supercapacitors," *RSC Adv.* 6(103), 101372-101379. DOI: 10.1039/C6RA22426A

He, F. (2010). "The pre-oxidation technology and device," in: *Carbon Fibre and Graphite Fibre (1st Ed.)*, Chemical Industry Press, Beijing, China, pp. 159-172.

Huang, Y., Ma, E., and Zhao, G. (2015). "Thermal and structure analysis on reaction mechanisms during the preparation of activated carbon fibers by KOH activation from liquefied wood-based fibers," *Ind. Crop. Prod.* 69, 447-455. DOI: 10.1016/j.indcrop.2015.03.002

Jin, Y. R., and Huang, Z. X. (2015). "Adsorption isotherms," in: *Adsorption and Pore Size Distribution (1st Ed.)*, National Defense Industry Press, Beijing, China, pp. 87-105.

Lastoskie, C., Gubbins, K. E., and Quirke, N. (1993). "Pore size distribution analysis of microporous carbon: A density functional theory approach," *J. Phys. Chem.-US* 97(18), 4786-4796. DOI: 10.1021/j100120a035

Li, X., Luo, X., Dou, L., and Chen, K. (2016). "Preparation and characterization of K_2CO_3-activated kraft lignin carbon," *BioResources* 11(1), 2096-2108. DOI: 10.15376/biores.11.1.2096-2108

Lin, J., and Zhao, G. (2016). "Preparation and characterization of high surface area activated carbon fibers from lignin," *Polymers-Basel* 8(10), 369-378. DOI: 10.3390/polym8100369

Lin, J., Shang, J.-B., and Zhao, G.-J. (2013). "The preparation and characterization of liquefied wood based primary fibers," *Carbohyd. Polym.* 91(1), 224-228. DOI: 10.1016/j.carbpol.2012.08.007

Liu, C.-j., Liang, X.-y., Teng, N., Liu, X.-j., Long, D.-h., Zhan, L., Zhang, R., Yang, J.-h., and Ling, L.-c. (2011). "The surface chemistry of pitch-based spherical activated carbon (PSAC) and the effect of gas-oxidation treatment on its adsorption performance," *Carbon* 25(6), 1808. DOI: 10.1016/j.carbon.2010.12.034

Liu, W., Wang, X., and Zhang, M. (2017). "Preparation of highly mesoporous wood-derived activated carbon fiber and the mechanism of its porosity development," *Holzforschung* 71(5), 363-371. DOI: 10.1515/hf-2016-0198

Liu, W., Zhang, Q., and Zhao, G. (2015). "Influence of activation time on the microstructure and antibacterial activity of nanosilver-containing activated carbon fibers prepared from liquefied wood," *Fiber. Polym.* 16(3), 522-528. DOI: 10.1007/s12221-015-0522-y

Liu, Y., Li, K., and Sun, G. (2010). "Effect of precursor preoxidation on the structure of phenolic resin-based activated carbon spheres," *J. Phys. Chem. Solids* 71(4), 453-456. DOI: 10.1016/j.jpcs.2009.12.009

Ma, C., Chen, X., Long, D., Wang, J., Qiao, W., and Ling, L. (2017). "High-surface-area and high-nitrogen-content carbon microspheres prepared by a pre-oxidation and mild KOH activation for superior supercapacitor," *Carbon* 118, 699-708. DOI: 10.1016/j.carbon.2017.03.075

Ma, X., and Zhao, G. (2010). "Preparation of carbon fibers from liquefied wood," *Wood Sci. Technol.* 44(1), 3-11. DOI: 10.1007/s00226-009-0264-3

Ma, X., and Zhao, G. (2011). "Variations in the microstructure of carbon fibers prepared from liquefied wood during carbonization," *J. Appl. Polym. Sci.* 121(6), 3525-3530. DOI: 10.1002/app.34142

Mangun, C. L., Benak, K. R., Economy, J., and Foster, K. L. (2001). "Surface chemistry, pore sizes and adsorption properties of activated carbon fibers and precursors treated with ammonia," *Carbon* 39(12), 1809-1820. DOI: 10.1016/S0008-6223(00)00319-5

Martín, C. F., Plaza, M. G., García, S., Pis, J. J., Rubiera, F., and Pevida, C. (2011). "Microporous phenol-formaldehyde resin-based adsorbents for pre-combustion CO_2 capture," *Fuel* 90(5), 2064-2072. DOI: 10.1016/j.fuel.2011.01.019

Nabais, J. M. V., Carrott, P. J. M., Carrott, M. M. L. R., and Menéndez, J. A. (2004). "Preparation and modification of activated carbon fibres by microwave heating," *Carbon* 42(7), 1315-1320. DOI: 10.1016/j.carbon.2004.01.033

Okada, K., Yamamoto, N., Kameshima, Y., and Yasumori, A. (2003). "Porous properties of activated carbons from waste newspaper prepared by chemical and physical activation," *J. Colloid Interf. Sci.* 262(1), 179-193. DOI: 10.1016/S0021-9797(03)00107-3

Pan, H., Shupe, T. F. and Hse, CY. (2009). "Characterization of novolac type liquefied wood/phenol/formaldehyde (LWPF) resin," *Eur. J. Wood Prod.* 67(4): 427-437. DOI: https://doi.org/10.1007/s00107-009-0337-x

Shang, J., Lin, J., Zhao, G., Zhang, J., Su, Z., and Guo, S. (2015). "Effects of time and chemical curing temperature on the properties of liquefied wood-based precursors and carbon fibers," *BioResources* 10(4), 7477-7488. DOI: 10.15376/biores.10.4.7477-7488

Shen, Z. M., Zhang, W. H., and Zhang, X. J. (2008). "Activated carbon microspheres," in: *Preparation and Application of Activated Carbon Materials*, 1st Ed., Chemical Industry Press, Beijing, China, pp. 127-131.

Silverstein, R. M., Webster, F. X., and Kiemle, D. J. (2005). "Infrared spectrometry," in: *Spectrometric Identification of Organic Compounds*, 7th Ed., Wiley, Hoboken, NJ, pp. 82-101.

Sun, Z.-l., Xi, L.-h., Li, H., Zeng, F.-l., and Lu, Y.-g. (2017). "Fourier transform infrared and dynamic thermomechanical analyses of mesophase pitch fibers during oxidative stabilization," *Carbon* 124, 727. DOI: 10.1016/j.carbon.2017.06.071

Wang, H., Shi, L., Yan, T., Zhang, J., Zhong, Q., and Zhang, D. (2014). "Design of graphene-coated hollow mesoporous carbon spheres as high performance electrodes for capacitive deionization," *J. Mater. Chem. A* 2(13), 4739-4750. DOI: 10.1039/C3TA15152B

Wickramaratne, N. P., and Jaroniec, M. (2013). "Importance of small micropores in CO_2 capture by phenolic resin-based activated carbon spheres," *J. Mater. Chem. A* 1(1), 112-116. DOI: 10.1039/C2TA00388K

Ye, C., Gong, Q.-M., Lu, F.-P., and Liang, J. (2008). "Preparation of carbon nanotubes/phenolic-resin-derived activated carbon spheres for the removal of middle molecular weight toxins," *Sep. Purif. Technol.* 61(1), 9-14. DOI: 10.1016/j.seppur.2007.09.021

Zhang, T., and Shen, Q. (2009). "Preparation and characterization of carbon fiber derived from lignin-phenol-formaldehyde resin," *J. Cellul. Sci. Technol.* 17(2), 6-11. DOI: 10.3969/j.issn.1004-8405.2009.02.002

Article submitted: June 25, 2018; Peer review completed: August 10, 2018; Revised version received: August 23, 2018; Accepted: August 24, 2018; Published: September 4, 2018.
DOI: 10.15376/biores.13.4.7983-7997